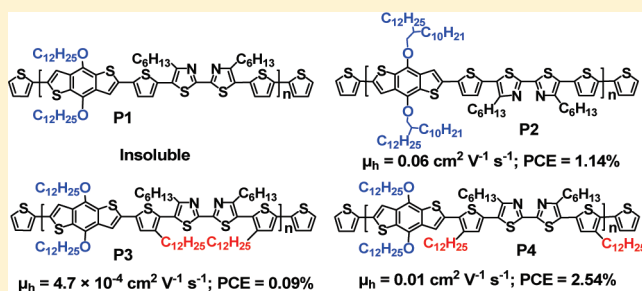


Side Chain Engineering of Copolymers Based on Bithiazole and Benzodithiophene for Enhanced Photovoltaic Performance

Qinqin Shi,^{†,‡} Haijun Fan,^{†,‡} Yao Liu,^{†,‡} Jianming Chen,^{†,‡} Lanchao Ma,^{†,‡} Wenping Hu,[†] Zhigang Shuai,[†] Yongfang Li,[†] and Xiaowei Zhan^{*,†}[†]Beijing National Laboratory for Molecular Sciences and CAS Key Laboratory of Organic Solids, Institute of Chemistry, Chinese Academy of Sciences, Beijing 100190, China[‡]Graduate University of Chinese Academy of Sciences, Beijing 100049, China

ABSTRACT: Four new copolymers **P1–P4** containing the same backbone of bithiazole acceptor unit and benzodithiophene donor unit but different side chain pattern were synthesized by Pd-catalyzed Stille coupling. The effect of the side chains on backbone conformation, solubility, absorption spectra, energy levels, charge transport, blend film morphology, and photovoltaic properties of the polymers were experimentally and theoretically investigated. The planarity of the main chain increases in the order **P3** < **P4** < **P1** ≈ **P2**. Upon increasing the planarity of the main chain, the polymer exhibits red-shifting of absorption maximum in film from 448 to 544 nm, upshifting of HOMO from -6.0 to -5.4 eV, downshifting of LUMO from -2.6 to -2.9 eV, and increasing of hole mobility from 4.7×10^{-4} to $0.06 \text{ cm}^2 \text{ V}^{-1} \text{ s}^{-1}$. Upon increasing the planarity of the polymer main chain, the phase separation size in polymer:PC₇₁BM blend increases. The polymer solar cells based on **P4**:PC₇₁BM (1:1, w/w) exhibit highest power conversion efficiency of 2.54% under AM 1.5, 100 mW cm^{-2} , which is attributed to combination of broad absorption, high mobility, and suitable phase separation benefited from moderate planarity of the main chain.



INTRODUCTION

Recently, polymer solar cells (PSCs) exhibit promising potential in the world's renewable energy strategy due to their unique advantages such as low cost, light weight, and large-area fabrication on flexible substrates and have attracted much attention.^{1–7} Through the creation of novel donor and acceptor materials and innovation of device fabrication technology, PSCs based on regioregular poly(3-hexylthiophene) (P3HT) have reached power conversion efficiencies (PCEs) over 6%,^{8–10} and PCEs of PSCs based on alternating copolymers have been over 7%.^{11–16} To further improve the PCE of PSCs, on one hand, electron donors and electron acceptors should have broad absorption, high mobility, and suitable energy levels; on the other hand, a better nanostructural ordering of donor and acceptor blends also facilitates charge generation and transport.

Thiazole is a widely used electron-accepting heterocycle due to electron-withdrawing nitrogen of imine (C=N). Small molecules and polymers based on bithiazole were used as semiconductors in organic field-effect transistors (OFETs) and exhibited high electron or hole mobility.^{17–20} Recently, conjugated copolymer-based bithiazoles have been used in PSCs as donors, and PCEs up to 3.82% were achieved in combination with PC₇₁BM acceptor.^{21–31} Most research work focused on main chain engineering of the bithiazole polymers, while there have been no reports on side chain engineering of the bithiazole polymers.

Long conjugation length, planar molecular geometry, and rigid structure in π -conjugated polymers often leads to poor solubility or even insoluble in common solvents. For solution processing, the use of long alkyl or alkoxy side chains has been a common approach to improve the solubility of conjugated polymers. However, the side chain nature and position not only affect the molecular weight, solubility, and geometry of the polymers but also affect the absorption, energy levels, and charge transport properties.^{32–42} Furthermore, the side chain affects morphology of resulting blends of polymer donors and fullerene acceptors, which has been regarded as a critical factor in determining the PCEs of the photovoltaic devices, and finally affects the photovoltaic performance of devices.^{12,43–51}

Here we demonstrate synthesis and characterization of four structural related copolymers of bithiazole and benzodithiophene with the same backbone but different side chain pattern (**P1–P4**, Figure 1). In particular, we probe into impact of the shape and position of side chains on solubility, absorption, energy levels, and charge transport properties of the polymers as well as on morphology and photovoltaic properties of the donor/acceptor blends. Tiny difference in the side chains of

Received: March 14, 2011

Revised: April 19, 2011

Published: May 05, 2011

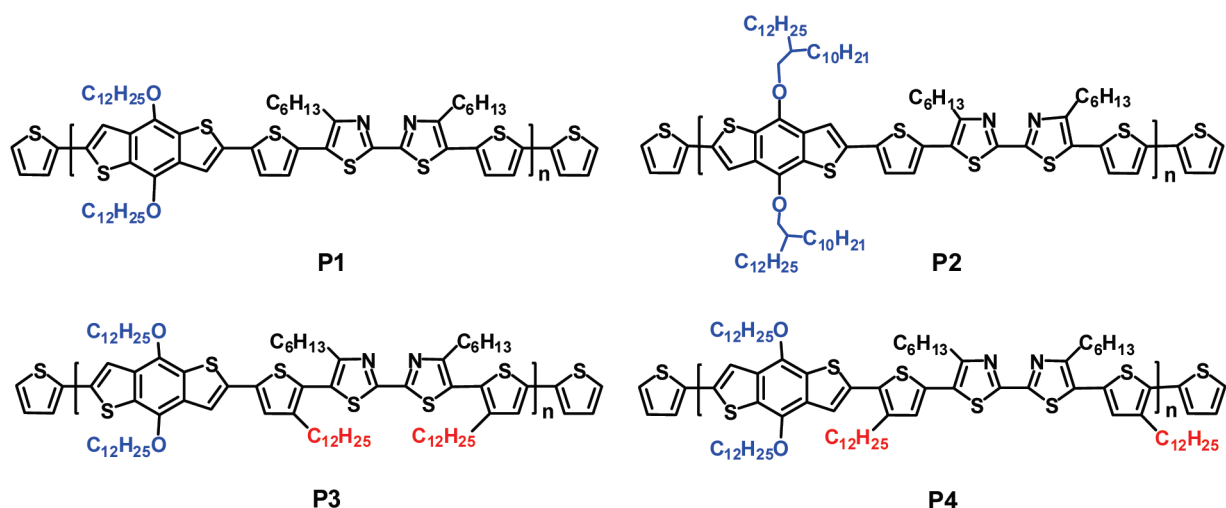


Figure 1. Chemical structures of polymers P1–P4.

P1–P4 leads to big difference in FET mobility (by a factor of ca. 130) and PSC efficiency (by a factor of ca. 30).

EXPERIMENTAL SECTION

Measurements and Characterization. The ^1H NMR and ^{13}C NMR spectra were measured on a Bruker AVANCE 400 MHz spectrometer using tetramethylsilane (TMS; $\delta = 0$ ppm) as an internal standard. Mass spectra (MALDI-TOF-MS) were determined on a Bruker BIFLEX III mass spectrometer. Elemental analyses were carried out using a FLASH EA1112 elemental analyzer. Thermogravimetric analysis (TGA) measurements were performed using a DTG-60 thermal analysis system under N_2 at a heating rate of $20^\circ\text{C min}^{-1}$. Solution (chloroform) and thin film (on quartz substrate) UV–vis spectra were recorded on a Jasco V-570 spectrophotometer. The electrochemical measurements were carried out under nitrogen on a deoxygenated solution of tetra-*n*-butylammonium hexafluorophosphate (0.1 M) in acetonitrile with a computer-controlled CHI660C electrochemical workstation, a glassy-carbon working electrode, a platinum-wire auxiliary electrode, and an Ag wire anodized with AgCl as a pseudoreference electrode. Potentials were referenced to the ferrocenium/ferrocene ($\text{FeCp}_2^{+/0}$) couple by using ferrocene as an internal standard. The gel permeation chromatography (GPC) measurements were performed on a Waters 515 chromatograph connected to a Waters 2414 refractive index detector, using THF as eluent and polystyrene standards as calibrants, and three Waters Styragel columns (HT2, -3, and -4) connected in series were used. The morphology of blend films was observed by an atomic force microscopy (AFM) (NanoMan VS, Veeco) in contact mode.

OFET Device Fabrication and Characterization. Field-effect transistors based on P2–P4 polymer films were fabricated in a bottom gate, top contact configuration at ambient atmosphere. Highly *n*-doped silicon and thermally grown silicon dioxide (300 nm) were used as back gate and gate dielectric, respectively. The substrates were cleaned with pure water, hot concentrated sulfuric acid–hydrogen peroxide solution (concentrated sulfuric acid/hydrogen peroxide water = 2:1), pure water, and pure isopropanol. Then vaporized octadecyltrichlorosilane (OTS) was used for surface modification of the gate dielectric layer.

Solutions of the polymers in *o*-dichlorobenzene (about 5 mg mL^{-1}) were spin-coated onto OTS treated substrates to form thin films. Prior to thermal evaporation of top contacts, the films were baked at 120°C in a vacuum chamber for 30 min to remove the residual solvent. Gold contacts (25 nm) for source and drain electrodes (finger parallel source-drain geometry) were vacuum-deposited at a rate of 1 \AA s^{-1} through a

metal shadow mask that defined a series of transistor devices with a channel length (L) of $50\text{ }\mu\text{m}$ and a channel width (W) of 1 mm. The characterization was accomplished by a Keithley 4200 SCS with a micromanipulator 6150 probe station in a clean shielded box at ambient atmosphere. Then field-effect mobility was calculated from the standard equation for saturation region in metal dioxide semiconductor field-effect transistors: $I_{\text{DS}} = (W/2L)\mu C_i(V_G - V_T)^2$, where I_{DS} is drain-source current, μ is field-effect mobility, W and L are the channel width and length, C_i is the capacitance per unit area of the dielectric layer ($C_i = 9.6\text{ nF cm}^{-2}$), V_G is the gate voltage, and V_T is the threshold voltage.

PSC Device Fabrication and Characterization. The PSC devices were fabricated with a structure of ITO/PEDOT:PSS/P2–P4:PC₇₁BM/Ca/Al. The patterned ITO glass (sheet resistance = $30\text{ }\Omega\text{ }\square^{-1}$) was pre-cleaned in an ultrasonic bath of acetone and isopropanol and treated in an ultraviolet-ozone chamber (Jelight Co.) for 30 min. A thin layer (30 nm) of poly(3,4-ethylenedioxythiophene):poly(styrenesulfonate) (PEDOT:PSS, Baytron P VP AI 4083, Germany) was spin-coated onto the ITO glass and baked at 120°C for 30 min. An *o*-dichlorobenzene solution of blend of P2 (P3 or P4)/PC₇₁BM (1:1, w/w) was subsequently spin-coated on the surface of PEDOT:PSS layer to form a photosensitive layer. Calcium (ca. 15 nm) and aluminum (ca. 50 nm) layers were subsequently evaporated onto the surface of the photosensitive layer in vacuum (ca. 10^{-5} Pa) to form the cathode. The active area of the device was 4 mm^2 . The current–voltage curve was measured with a computer-controlled Keithley 236 Source Measure Unit. A xenon lamp coupled with AM 1.5 solar spectrum filters was used as the light source, and the optical power at the sample was 100 mW cm^{-2} . The incident photon-to-current conversion efficiency (IPCE) spectrum was measured by a Stanford Research Systems model SR830 DSP lock-in amplifier coupled with WDG3 monochromator and a 500 W xenon lamp.

Materials. 4,8-Dihydrobenzo[1,2-*b*:4,5-*b'*]dithiophen-4,8-dione,⁵² 2,6-bis(trimethyltin)-4,8-didodecyloxybenzo[1,2-*b*:4,5-*b'*]dithiophene (8),⁵² 2-bromo-3-dodecylthiophene,⁵³ (4-dodecylthiophen-2-yl)trimethylstannane,⁵³ 5,5'-dibromo-4,4'-dihexyl-2,2'-bi-1,3-thiazole,²¹ 5,5'-bis(5-bromothiophen-2-yl)-4,4'-dihexyl-2,2'-bithiazole (7),²⁸ and 5,5'-bis(trimethyltin)-4,4'-dihexyl-2,2'-bithiazole²⁹ were synthesized according to the literature methods. Toluene and THF were distilled from sodium benzophenone under nitrogen before use. Bio-Rad Bio-Beads S-X1 is a kind of porous cross-linked polystyrene polymers used for gel permeation separations of lipophilic polymers and low molecular weight, hydrophobic materials in the presence of organic solvents. Unless stated

otherwise, the other reagents were purchased from commercial sources and used without further purification.

4,8-Di(2-decyltetradecyloxy)benzo[1,2-*b*:4,5-*b'*]dithiophene (1). 4,8-Dihydrobenzo[1,2-*b*:4,5-*b'*]dithiophen-4,8-dione (220 mg, 1 mmol), zinc powder (143 mg, 2.2 mmol), and 5 mL of water were put into a 25 mL flask; then NaOH (600 mg, 15 mmol) was added into the mixture. The mixture was stirred at reflux for 1 h. Then, 11-(bromomethyl)tricosane (1.3 g, 3 mmol) and tetrabutylammonium bromide (TBAB) (49 mg, 0.15 mmol) were added into the flask. After stirring at reflux for 8 h, the mixture was poured into cold water and extracted with diethyl ether (100 mL \times 2). The ether layer was dried over anhydrous MgSO₄. After concentration, the residue was purified by column chromatography (silica gel, hexane) to afford yellow oil (660 mg, 74%). ¹H NMR (400 MHz, CDCl₃): δ 7.48 (d, *J* = 5.5 Hz, 2H), 7.36 (d, *J* = 5.5 Hz, 2H), 4.17 (d, *J* = 5.2 Hz, 4H), 1.87 (m, 2H), 1.64 (m, 4H), 1.49–1.27 (m, 76H), 0.88 (m, 12H). ¹³C NMR (100 MHz, CDCl₃): δ 144.83, 131.66, 130.09, 125.98, 120.41, 39.40, 32.14, 31.52, 30.27, 29.90, 29.88, 29.58, 27.19, 22.90, 14.30. MS (MALDI): *m/z* 895 (M⁺). Anal. Calcd for C₅₈H₁₀₂O₂S₂: C, 77.79; H, 11.48. Found: C, 77.87; H, 11.36%.

2,6-Bis(trimethyltin)-4,8-di(2-decyltetradecyloxy)benzo[1,2-*b*:4,5-*b'*]dithiophene (2). A solution of **1** (894 mg, 1 mmol) in 17 mL of dry THF was deoxygenated with nitrogen, and a 2.5 M solution of *n*-butyllithium in hexane (1.4 mL, 3.5 mmol) was added dropwise at room temperature. After the solution was stirred at room temperature for 1 h, trimethyltin chloride (478 mg, 2.4 mmol) (*caution: very toxic!*) was added in one portion. The mixture was stirred at ambient temperature for 2 h. Then, the mixture was poured into 200 mL of cool water and extracted with diethyl ether. The organic layer was washed with water and then dried over anhydrous MgSO₄. After the solvent was removed under vacuum, the residue was recrystallized from acetone twice to give a white solid (855 mg, 70%). ¹H NMR (400 MHz, CDCl₃): δ 7.50 (s, 2H), 4.17 (d, *J* = 5.0 Hz, 4H), 1.87 (m, 2H), 1.64 (m, 4H), 1.49–1.26 (m, 76H), 0.88 (m, 12H), 0.44 (s, 18H). ¹³C NMR (100 MHz, CDCl₃): δ 143.30, 140.37, 133.91, 132.96, 128.03, 39.27, 31.99, 31.48, 30.25, 29.83, 29.79, 29.75, 29.43, 27.14, 22.75, 14.17, –8.32. Anal. Calcd for C₆₄H₁₁₈O₂S₂Sn₂: C, 62.95; H, 9.74. Found: C, 64.24; H, 9.89%.

5,5'-Bis(3-dodecylthiophen-2-yl)-4,4'-dihexyl-2,2'-bithiazole (3). 5,5'-Bis(trimethyltin)-4,4'-dihexyl-2,2'-bithiazole (1.56 g, 3 mmol) and 2-bromo-3-dodecylthiophene (2.97 g, 9 mmol) were dissolved in 55 mL of anhydrous toluene and deoxygenated with N₂ for 30 min. Then, Pd(PPh₃)₄ (347 mg, 0.3 mmol) was added under N₂. The mixture was stirred at reflux for 1 day. Then, the mixture was poured into water, extracted with dichloromethane, and dried over anhydrous MgSO₄. After concentration, the residue was purified by column chromatography (silica gel, hexane) to afford yellow oil (790 mg, 31%). ¹H NMR (400 MHz, CDCl₃): δ 7.35 (d, *J* = 5.2 Hz, 2H), 7.00 (d, *J* = 5.2 Hz, 2H), 2.69 (t, *J* = 7.6 Hz, 4H), 2.55 (t, *J* = 7.6 Hz, 4H), 1.71 (m, 4H), 1.56 (m, 4H), 1.24 (m, 48H), 0.86 (m, 12H). ¹³C NMR (100 MHz, CDCl₃): δ 160.39, 157.53, 143.58, 129.03, 126.36, 126.45, 32.07, 31.74, 30.78, 29.90, 29.78, 29.75, 29.71, 29.60, 29.58, 29.49, 29.21, 29.09, 22.84, 22.73, 14.26, 14.21. MS (MALDI): *m/z* 837 (M⁺). Anal. Calcd for C₅₀H₈₀N₂S₄: C, 71.71; H, 9.63; N, 3.35. Found: C, 71.55; H, 9.55; N, 3.20%.

5,5'-Bis(5-bromo-3-dodecylthiophen-2-yl)-4,4'-dihexyl-2,2'-bithiazole (4). Compound **3** (251 mg, 0.3 mmol) was dissolved in a mixture of chloroform (2 mL) and glacial acetic acid (0.4 mL). NBS (112 mg, 0.63 mmol) was then added to the solution and stirred for 2 h in the dark. Then, the mixture was poured into water, extracted with dichloromethane, and dried over anhydrous MgSO₄. After concentration, the residue was purified by column chromatography (silica gel, hexane) to afford yellow oil (135 mg, 45%). ¹H NMR (400 MHz, CDCl₃): δ 6.96 (s, 2H), 2.67 (t, *J* = 7.6 Hz, 4H), 2.47 (t, *J* = 7.6 Hz, 4H), 1.69 (m, 4H), 1.52 (m, 4H), 1.25 (m, 48H), 0.86 (m, 12H). ¹³C NMR (100 MHz, CDCl₃): δ 160.61, 158.13, 144.46, 131.86, 126.82, 124.26, 113.15,

32.07, 31.75, 30.59, 29.89, 29.77, 29.73, 29.66, 29.54, 29.49, 29.47, 29.20, 29.07, 22.84, 22.73, 14.27, 14.22. MS (MALDI): *m/z* 995 (M⁺). Anal. Calcd for C₅₀H₇₈N₂S₄Br₂: C, 60.34; H, 7.90; N, 2.81. Found: C, 60.18; H, 7.92; N, 2.76%.

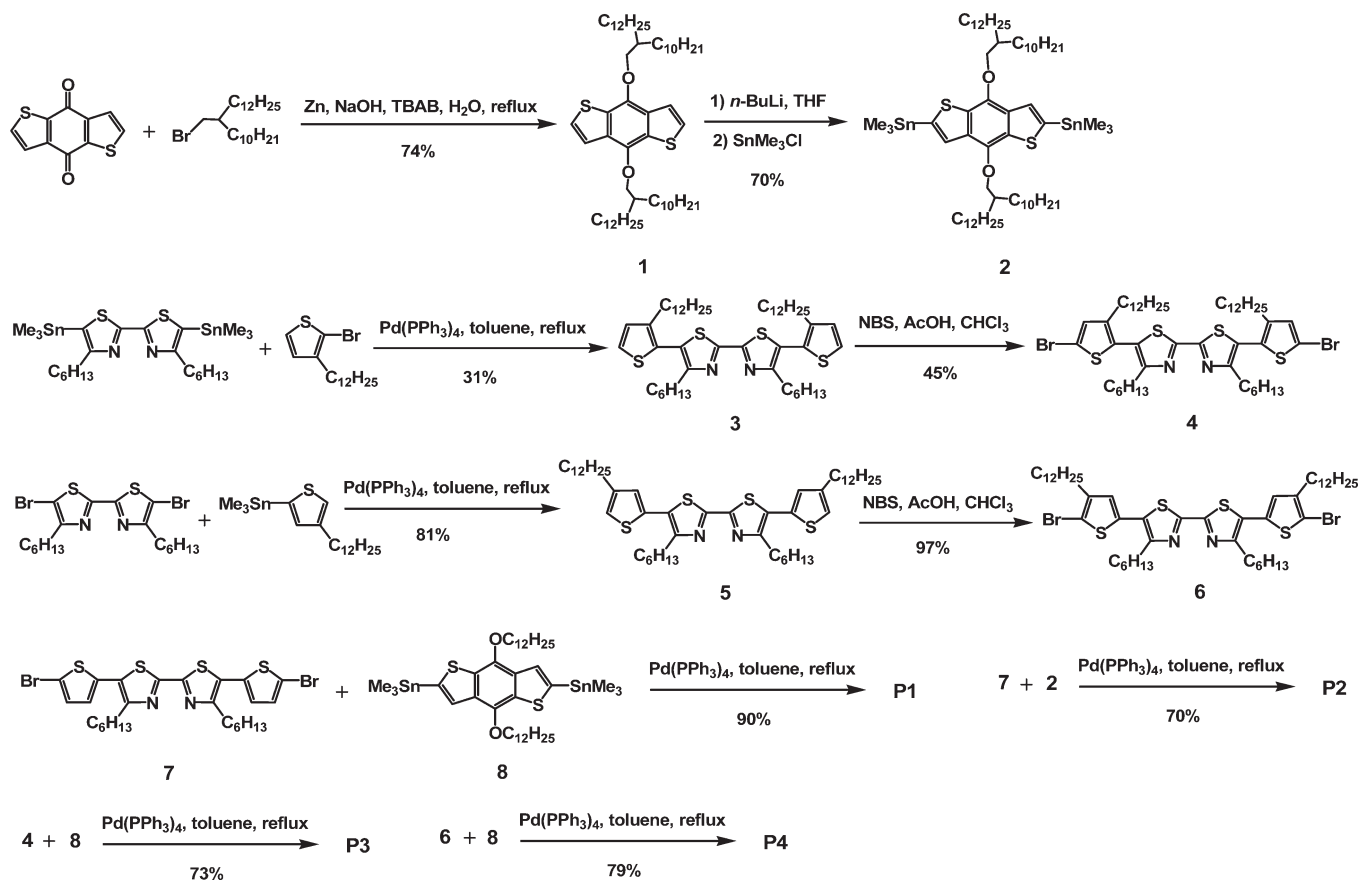
5,5'-Bis(4-dodecylthiophen-2-yl)-4,4'-dihexyl-2,2'-bithiazole (5). 5,5'-Dibromo-4,4'-dihexyl-2,2'-bithiazole (494 mg, 1 mmol) and (4-dodecylthiophen-2-yl)trimethylstannane (1.623 g, 4 mmol) were dissolved in 15 mL of anhydrous toluene and deoxygenated with N₂ for 30 min. Then, Pd(PPh₃)₄ (115 mg, 0.1 mmol) was added under N₂. The mixture was stirred at reflux for 1 day. Then, the mixture was poured into water, extracted with dichloromethane, and dried over anhydrous MgSO₄. After concentration, the residue was purified by column chromatography (silica gel, hexane) to afford yellow oil (677 mg, 81%). ¹H NMR (400 MHz, CDCl₃): δ 7.03 (s, 2H), 6.95 (s, 2H), 2.94 (t, *J* = 7.7 Hz, 4H), 2.62 (t, *J* = 7.6 Hz, 4H), 1.79 (m, 4H), 1.63 (m, 4H), 1.42–1.28 (m, 48H), 0.88 (m, 12H). ¹³C NMR (100 MHz, CDCl₃): δ 157.69, 154.39, 144.14, 132.81, 128.85, 128.05, 121.25, 32.07, 31.78, 30.54, 30.51, 29.83, 29.75, 29.62, 29.56, 29.51, 29.45, 29.32, 22.84, 22.77, 14.25, 14.23. MS (MALDI): *m/z* 837 (M⁺). Anal. Calcd for C₅₀H₈₀N₂S₄: C, 71.71; H, 9.63; N, 3.35. Found: C, 71.52; H, 9.59; N, 3.31%.

5,5'-Bis(5-bromo-4-dodecylthiophen-2-yl)-4,4'-dihexyl-2,2'-bithiazole (6). Compound **5** (418 mg, 0.5 mmol) was dissolved in a mixture of chloroform (2.5 mL) and glacial acetic acid (0.6 mL). NBS (190 mg, 1.1 mmol) was then added to the solution and stirred for 2 h in the dark. Then, the mixture was poured into water, extracted with dichloromethane, and dried over anhydrous MgSO₄. After concentration, the residue was purified by column chromatography (silica gel, hexane) to afford yellow oil (480 mg, 97%). ¹H NMR (400 MHz, CDCl₃): δ 6.87 (s, 2H), 2.88 (t, *J* = 7.7 Hz, 4H), 2.57 (t, *J* = 7.6 Hz, 4H), 1.76 (m, 4H), 1.60 (m, 4H), 1.33–1.26 (m, 48H), 0.88 (m, 12H). ¹³C NMR (100 MHz, CDCl₃): δ 157.89, 154.88, 143.00, 132.60, 128.41, 127.30, 110.17, 32.10, 31.77, 30.52, 29.84, 29.79, 29.75, 29.66, 29.59, 29.54, 29.39, 29.31, 22.86, 22.82, 22.79, 14.25. MS (MALDI): *m/z* 995 (M⁺). Anal. Calcd for C₅₀H₇₈N₂S₄Br₂: C, 60.34; H, 7.90; N, 2.81. Found: C, 60.34; H, 7.94; N, 2.86%.

Poly{(4,8-didodecyloxybenzodithiophene-2,6-diyl)-alt-[5,5'-bis(2-thienyl)-4,4'-dihexyl-2,2'-bithiazole-5,5'-diyl]} (**P1**). **8** (89 mg, 0.1 mmol) and **7** (66 mg, 0.1 mmol) were dissolved in 10 mL of anhydrous toluene and deoxygenated with N₂ for 30 min. Pd(PPh₃)₄ (11.5 mg, 0.01 mmol) was then added under N₂. The mixture was stirred at reflux for 3 days. To end-cap the polymer chain, tributyl(thiophen-2-yl)stannane (3.7 mg, 0.01 mmol) was added under nitrogen, and the mixture was stirred at reflux for 10 h. 2-Bromothiophene (3.3 mg, 0.02 mmol) was then added under nitrogen, and the mixture was stirred at reflux for 10 h. After the reaction mixture was cooled to room temperature, the polymer was precipitated by addition of 80 mL of methanol. The precipitate was filtered as a purple solid (95 mg, 90%). We did not take any purification and measurements due to very bad solubility in common organic solvents.

Poly{(4,8-didodecyltetradecyloxybenzodithiophene-2,6-diyl)-alt-[5,5'-bis(2-thienyl)-4,4'-dihexyl-2,2'-bithiazole-5,5'-diyl]} (**P2**). **2** (183 mg, 0.15 mmol) and **7** (99 mg, 0.15 mmol) were dissolved in 15 mL of anhydrous toluene and deoxygenated with N₂ for 30 min. Pd(PPh₃)₄ (18 mg, 0.015 mmol) was then added under N₂. The mixture was stirred at reflux for 3 days. To end-cap the polymer chain, tributyl(thiophen-2-yl)stannane (5.5 mg, 0.015 mmol) was added under nitrogen, and the mixture was stirred at reflux for 10 h. 2-Bromothiophene (5 mg, 0.03 mmol) was then added under nitrogen, and the mixture was stirred at reflux for 10 h. After the reaction mixture was cooled to room temperature, the polymer was precipitated by addition of 80 mL of methanol. The precipitate was filtered. Finally, the polymer was purified by size exclusion column chromatography over Bio-Rad Bio-Beads S-X1 eluting with chloroform. The polymer was recovered as a purple solid

Scheme 1. Synthetic Routes of the Polymers



from the chloroform fraction by rotary evaporation (150 mg, 70%). ^1H NMR (400 MHz, CDCl_3): δ 7.40 (br, 2H), 7.07 (br, 4H), 4.16 (br, 4H), 2.99 (br, 4H), 1.84–1.26 (br, 98H), 0.88 (br, 18H). GPC: M_n 8750; M_w 11 804; M_w/M_n 1.3. Anal. Calcd for $(\text{C}_{84}\text{H}_{130}\text{N}_2\text{O}_2\text{S}_6)_n$: C, 72.46; H, 9.41; N, 2.01. Found: C, 70.71; H, 9.32; N, 2.00%.

Poly{(4,8-didodecyloxybenzodithiophene-2,6-diyl)-alt-[5,5'-bis(3-dodecylthiophen-2-yl)-4,4'-dihexyl-2,2'-bithiazole-5,5'-diyl]} (**P3**). **8** (80 mg, 0.091 mmol) and **4** (90 mg, 0.091 mmol) were dissolved in 10 mL of anhydrous toluene and deoxygenated with N_2 for 30 min. $\text{Pd}(\text{PPh}_3)_4$ (11.5 mg, 0.01 mmol) was then added under N_2 . The mixture was stirred at reflux for 3 days. To end-cap the polymer chain, tributyl(thiophen-2-yl)stannane (3.7 mg, 0.01 mmol) was added under nitrogen, and the mixture was stirred at reflux for 10 h. 2-Bromothiophene (3.3 mg, 0.02 mmol) was then added under nitrogen, and the mixture was stirred at reflux for 10 h. After the reaction mixture was cooled to room temperature, the polymer was precipitated by addition of 80 mL of methanol. The precipitate was filtered. Finally, the polymer was purified by size exclusion column chromatography over Bio-Rad Bio-Beads S-X1 eluting with chloroform. The polymer was recovered as a purple solid from the chloroform fraction by rotary evaporation (99 mg, 73%). ^1H NMR (400 MHz, CDCl_3): δ 7.49 (br, 2H), 7.19 (br, 2H), 4.24 (br, 4H), 2.69 (br, 4H), 2.50 (br, 4H), 1.85 (br, 4H), 1.68 (br, 4H), 1.53 (br, 4H), 1.19 (br, 84H), 0.80 (br, 18H). GPC: M_n 7489; M_w 11 652; M_w/M_n 1.5. Anal. Calcd for $(\text{C}_{84}\text{H}_{130}\text{N}_2\text{O}_2\text{S}_6)_n$: C, 72.46; H, 9.41; N, 2.01. Found: C, 68.42; H, 9.01; N, 1.97%.

Poly{(4,8-didodecyloxybenzodithiophene-2,6-diyl)-alt-[5,5'-bis(4-dodecylthiophen-2-yl)-4,4'-dihexyl-2,2'-bithiazole-5,5'-diyl]} (**P4**). **8** (177 mg, 0.2 mmol) and **6** (199 mg, 0.2 mmol) were dissolved in 10 mL of anhydrous toluene and deoxygenated with N_2 for 30 min.

$\text{Pd}(\text{PPh}_3)_4$ (23 mg, 0.02 mmol) was then added under N_2 . The mixture was stirred at reflux for 3 days. To end-cap the polymer chain, tributyl(thiophen-2-yl)stannane (7.4 mg, 0.02 mmol) was added under nitrogen, and the mixture was stirred at reflux for 10 h. 2-Bromothiophene (6.6 mg, 0.04 mmol) was then added under nitrogen, and the mixture was stirred at reflux for 10 h. After the reaction mixture was cooled to room temperature, the polymer was precipitated by addition of 80 mL of methanol. The precipitate was filtered. Finally, the polymer was purified by size exclusion column chromatography over Bio-Rad Bio-Beads S-X1 eluting with chloroform. The polymer was recovered as a purple solid from the chloroform fraction by rotary evaporation (220 mg, 79%). ^1H NMR (400 MHz, CDCl_3): δ 7.49 (br, 2H), 7.09 (br, 2H), 4.33 (br, 4H), 2.90 (br, 4H), 2.80 (br, 4H), 1.92 (br, 4H), 1.84 (br, 4H), 1.75 (br, 4H), 1.25–1.35 (br, 84H), 0.98 (br, 18H). GPC: M_n 6933; M_w 9805; M_w/M_n 1.4. Anal. Calcd for $(\text{C}_{84}\text{H}_{130}\text{N}_2\text{O}_2\text{S}_6)_n$: C, 72.46; H, 9.41; N, 2.01. Found: C, 72.15; H, 9.26; N, 2.04%.

RESULTS AND DISCUSSION

Synthesis and Characterization. Scheme 1 shows the synthetic routes to the monomers and polymers. Monomer **2** was synthesized using similar methods to monomer **8** reported in the literature. Monomers **4** and **6** were synthesized by Stille coupling of bithiazole dinitrile (or dibromide) with thiophene bromide (or tin), followed by bromination with NBS. Polymers **P1**–**P4** were synthesized by Stille coupling copolymerization of benzodithiophene dinitrile with 5,5'-bis(thiophen-2-yl)bithiazole dibromide. Because of the coplanar structure and strong interchain

interaction of the backbone, **P1** was insoluble, and we did not measure their properties. Replacing *n*-dodecyl on benzodithiophene with 2-decyltetradecyl branched group (**P2**) or introducing *n*-dodecyl onto thiophene (**P3**, **P4**) significantly enhances solubility of **P1**. Thus, **P2–P4** are soluble in common organic solvents such as chloroform, THF, and dichlorobenzene.

Molecular weights of the polymers were determined by gel permeation chromatography (GPC) using polystyrene standards as calibrants (Table 1). The number-average molecular weights (M_n) of **P2–P4** are 8750, 7489, and 6933, with a polydispersity index (M_w/M_n) of 1.3, 1.5, and 1.4, respectively. The thermal properties of the polymers were determined by thermogravimetric analysis (TGA) under nitrogen (Figure 2). **P2–P4** show good thermal stability with similar decomposition temperature over 320 °C (Table 1).

Table 1. Molecular Weights and Thermal Data of Copolymers P2–P4

polymer	yield (%)	M_n^a	M_w^a	M_w/M_n^a	T_d^b (°C)
P2	70	8750	11 804	1.3	326
P3	73	7489	11 652	1.5	328
P4	79	6933	9 805	1.4	328

^a Number-average molecular weight (M_n), weight-average molecular weight (M_w), and polydispersity index (M_w/M_n) were measured by GPC using THF as an eluent and polystyrene as a standard. ^b Temperature at 5% weight loss measured by TGA at a heating rate of 20 °C min⁻¹ under nitrogen.

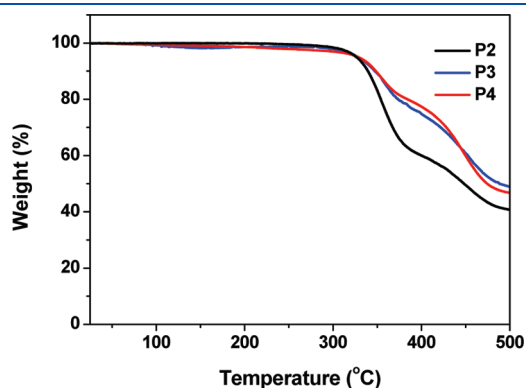


Figure 2. TGA curves of polymers **P2–P4**.

Optical Properties. The absorption spectra of copolymers **P2–P4** in chloroform solutions (10⁻⁶ M) and in thin solid films are shown in Figure 3. In solution, the absorption maxima of **P2–P4** are 484, 426, and 464 nm, respectively (Table 2). **P2** exhibits the longest absorption maximum due to its planar structure of the main chain, while **P3** exhibits the shortest absorption maximum due to the twisted structure of the main chain (see theory calculation below). Because of the strong π – π interchain association and aggregation, the absorption maximum of **P2** and **P4** in the film red shifts 56–60 nm relative to that in solution, which is larger than that of **P3** (22 nm). Especially for **P2**, the shoulder peak at 580 nm is the characteristics of the self-assembly of the polymer.⁵⁴ The bandgaps of **P2–P4**, estimated from the onset edge of absorption spectra in solid films, are 1.93, 1.99, and 1.94 eV, respectively.

Electrochemical Properties. Cyclic voltammograms of the polymers **P2–P4** are illustrated in Figure 4. Apparently, they show similar profiles with one irreversible oxidation peak and one irreversible reduction peak. The HOMO and LUMO values of **P2–P4** are estimated from the onset oxidation and reduction potential, assuming the absolute energy level of FeCp₂^{+ / 0} to be 4.8 eV below vacuum⁵⁵ (Table 2). As the π -electrons are prone to delocalize in the planar structure and to localize in the twisted structure, **P2** and **P4** exhibit higher HOMO and lower LUMO, while **P3** exhibits lower HOMO and higher LUMO. The trend in the electrochemical data is consistent with the trend in the absorption maxima and theory calculation (see below). Since open-circuit voltage (V_{oc}) of PSCs is generally linearly correlated with the difference between the HOMO level of electron donor and the LUMO level of electron acceptor, the low HOMO levels (–5.4 to –6.0 eV) of **P2–P4** could result in high V_{oc} .

Table 2. Absorption Data and Energy Levels of P2–P4

polymer	λ_{max}^a (nm)		E_g^{optb} (eV)	HOMO ^c (eV)	LUMO ^c (eV)
	solution	film			
P2	484	544	1.93	–5.50	–2.83
P3	426	448	1.99	–5.95	–2.63
P4	464	520	1.94	–5.48	–2.92

^a Absorption maxima. ^b Optical bandgap estimated from the onset edge of absorption spectra in solid film. ^c HOMO and LUMO estimated from the onset oxidation and reduction potentials, respectively, assuming the absolute energy level of ferrocene/ferrocenium to be 4.8 eV below vacuum.

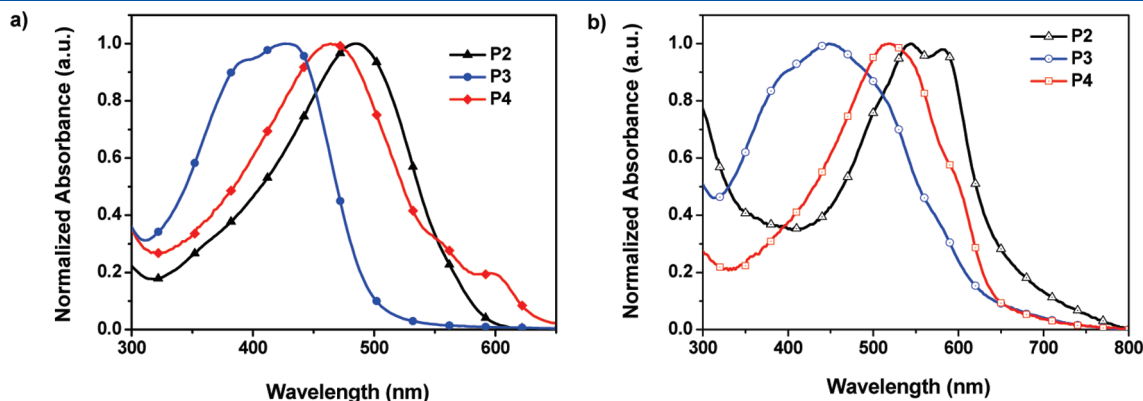


Figure 3. Absorption spectra of **P2–P4** in chloroform (a) and in thin film (b).

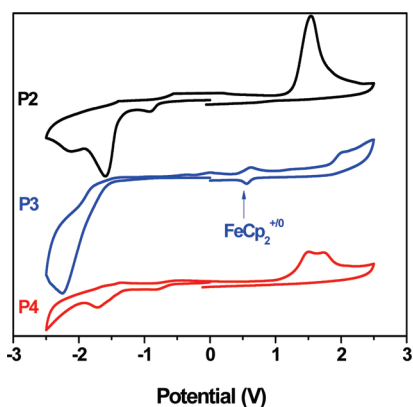


Figure 4. Cyclic voltammograms for **P2–P4** in $\text{CH}_3\text{CN}/0.1 \text{ M } [^n\text{Bu}_4\text{N}]^+[\text{PF}_6]^-$ with ferrocenium/ferrocene as an internal standard, at 50 mV s^{-1} . The horizontal scale refers to an anodized Ag wire pseudoreference electrode.

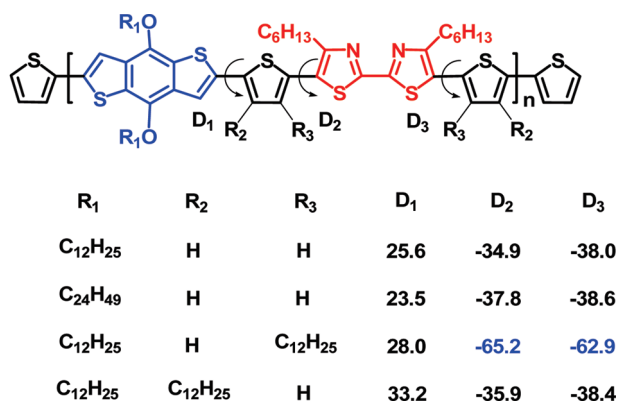


Figure 5. Several key dihedral angles of the polymers.

Calculation. To provide an insight into the molecular architecture of the polymers, molecular simulation was carried out for **P1–P4** with a chain length of $n = 1$ using density functional theory (DFT) at the B3LYP/6-31G (d,p) level^{56,57} with Gaussian 09 program package.⁵⁸ Dihedral angles between benzodithiophene and thiophene (D_1) and between thiophene and thiazole (D_2 and D_3) (Figure 5) are susceptible to the substituents on thiophenes and benzodithiophene. The dihedral angles (D_2 , D_3) between thiophene and thiazole (head-to-tail coupling) in **P1**, **P2**, and **P4** are 35° – 39° , much smaller than those (63° – 65°) in **P3** (head-to-head coupling). Dihedral angle between benzodithiophene and thiophene (D_1) in **P1** and **P2** is smaller than that in **P3** and **P4** due to absence of the substituent on the adjacent thiophene, while D_1 in **P4** is the largest due to 3-dodecyl group on the adjacent thiophene. Thus, **P1** and **P2** have most planar main chain, **P4** has more planar main chain, while **P3** has most twisted main chain. The most planar conformation of the main chain leads to strong interchain interaction and poor solubility of **P1**.

The absorption spectra of the polymers are related to the geometry of their backbone, which can be defined by the dihedral angles. The absorption maxima of the polymers shift to longer wavelengths in the order of $\text{P3} < \text{P4} < \text{P2}$, consistent with their dihedral angle profile. **P3** with the largest dihedral angles shows the shortest absorption maxima. The smallest red shift of

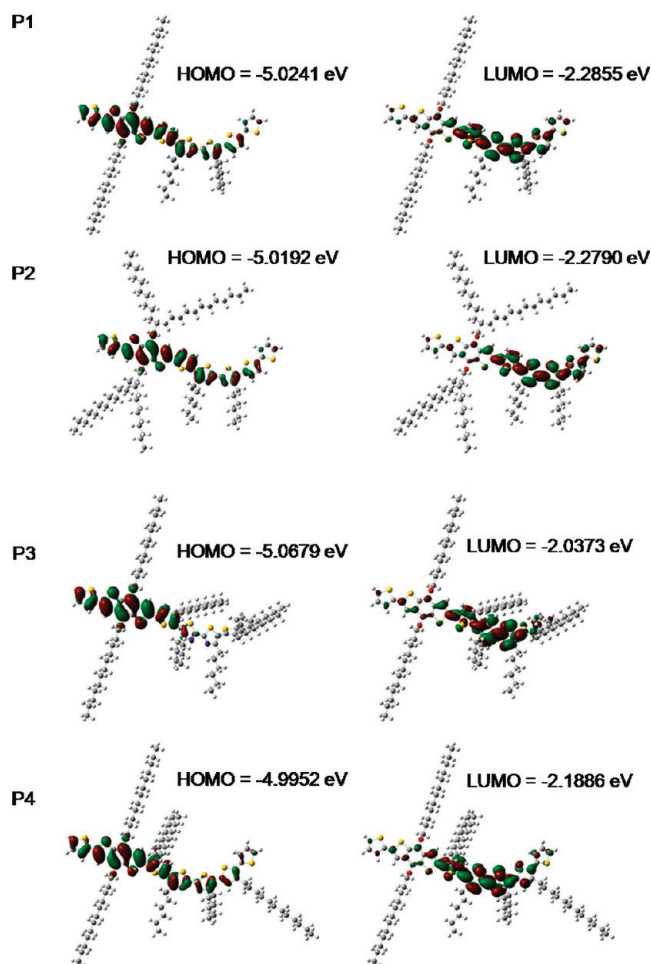


Figure 6. Molecular orbital geometry and energy levels obtained from DFT calculations on **P1–P4** with a chain length $n = 1$ at the B3LYP/6-31G* level.

Table 3. OFET Characteristics of **P2–P4** in Air

polymer	μ_{h} ($\text{cm}^2 \text{V}^{-1} \text{s}^{-1}$)	$I_{\text{on}}/I_{\text{off}}$	V_{T} (V)
P2	0.06	2000	5
P3	4.7×10^{-4}	314	-17
P4	0.01	10^4	-2

absorption from solution to thin film suggests that the π – π stacking among the polymer chains is limited due to the highly twisted structure of the main chain in **P3**.

Figure 6 shows the calculated molecular orbital geometry and energy levels of the polymers. Because of the twisted main chain of **P3**, the HOMO is located on the benzodithiophene and adjacent thiophenes, while the HOMOs in **P1**, **P2**, and **P4** are delocalized over the polymer backbones. As a result, the HOMO of **P3** is lower than those in **P1**, **P2**, and **P4**. Because of the same origin, the LUMO of **P3** is more localized and higher than those in **P1**, **P2**, and **P4**. The calculation is in considerable coincidence with electrochemistry. Thus, it is clear that the side chains on thiophene can be used as a tuning means to control the torsional angle and, therefore, to control the electronic and optical properties of the polymers.

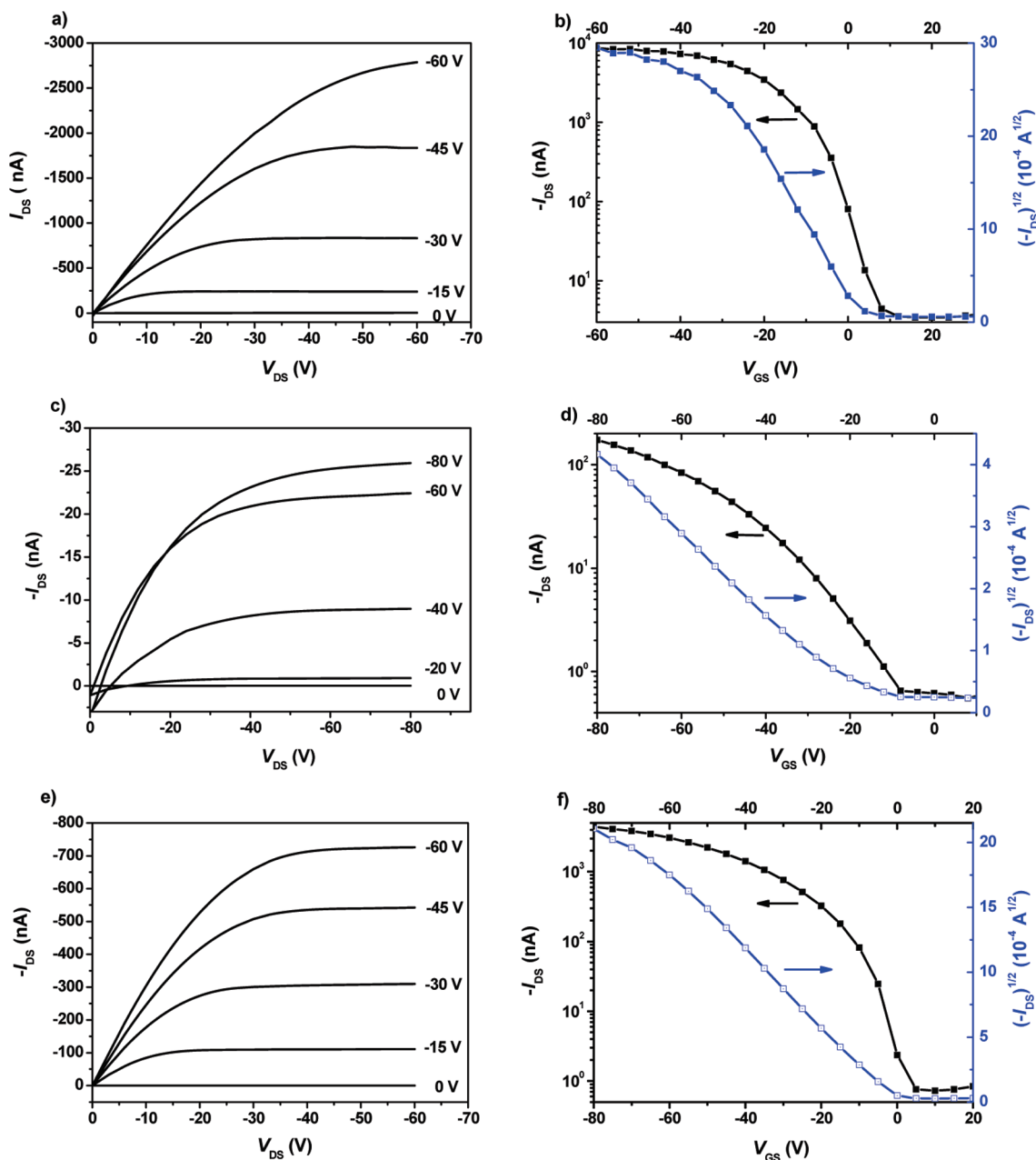


Figure 7. Typical current–voltage characteristics (I_{DS} vs V_{DS}) at different gate voltages (V_{GS}) and $-I_{DS}$ and $(-I_{DS})^{1/2}$ vs V_{GS} plots at V_{DS} of -100 V for a top contact device based on **P2** (a, b), **P3** (c, d), and **P4** (e, f).

Organic Field-Effect Transistors. OFET devices were fabricated in a top-contact configuration using Au as source and drain electrodes to study charge transport properties of these polymers. The results from optimized OFETs for each polymer are summarized in Table 3. Typical output and transfer characteristics of OFET devices are shown in Figure 7. Three polymers exhibited typical p-type semiconductor behavior in air. Because of the planar structure of main chain and strong interchain interactions, the devices based on **P2** and **P4** exhibit higher hole mobility of 0.06 and 0.01 $\text{cm}^2 \text{V}^{-1} \text{s}^{-1}$, respectively. The hole mobilities of **P2** and **P4** are among the top values reported for photovoltaic polymers.⁷ Because of the twisted backbone, the mobility of device based **P3** shows 2 orders of magnitude lower than those of **P2** and **P4**. Although these polymers have an

identical backbone, the tiny difference in the side chains leads to huge difference in charge transport.

Photovoltaic Properties. To demonstrate potential applications of these polymers in PSCs, we used **P2–P4** as an electron donor and PC_{71}BM as an electron acceptor⁵⁹ and fabricated bulk heterojunction PSCs with a structure of ITO/PEDOT:PSS/**P2**(**P3** or **P4**): PC_{71}BM (1:1, w/w)/Ca/Al. Figure 8 shows current density–voltage curves, and Table 4 summarizes the open circuit voltage (V_{oc}), short circuit current density (J_{sc}), fill factor (FF), and the power conversion efficiency (PCE) of the devices. The PCEs of **P2**-, **P3**-, and **P4**-based devices are 1.14, 0.09, and 2.54%, respectively. The very low PCE of **P3**-based device is attributed to narrow absorption and low mobility. To our surprise, **P2** exhibits better absorption and higher mobility

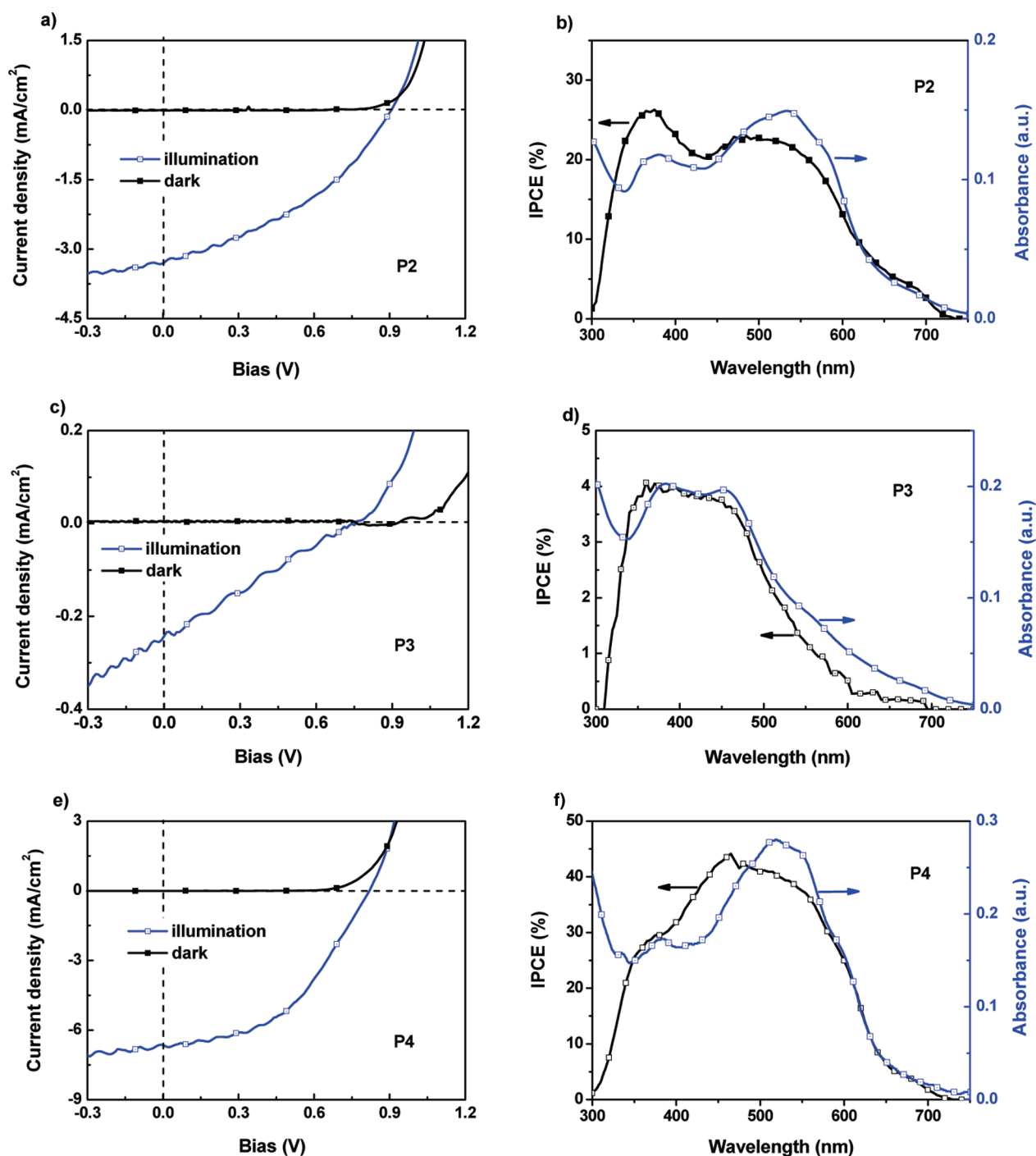


Figure 8. Current density–voltage characteristics of devices with the structure ITO/PEDOT:PSS/P2 (P3 or P4):PC₇₁BM (1:1, w/w)/Ca/Al (left) and corresponding absorption spectrum of a film of P2(P3 or P4):PC₇₁BM blend and IPCE as a function of wavelength under the illumination of an AM 1.5 solar simulator, 100 mW cm⁻² (right).

than P4, but the PCE of P2-based device is only half of that of P4-based device.

The open-circuit voltages (V_{oc}) of the PSCs based on P2–P4 are relatively high (0.76–0.91 V) due to low HOMO levels of the polymers. The HOMO level of P3 is the lowest, so the V_{oc} of P3-based PSCs is supposed to be the highest. However, the V_{oc} is the smallest. In addition to the difference between the LUMO of PC₇₁BM and the HOMO of polymer donor, mobility and morphology of the active layer also need to be taken into account

for V_{oc} .^{2,60–62} For P3, the lowest V_{oc} is most likely attributed to charge recombination losses at the polymer/fullerene interfaces and at the electrodes due to low mobility (4.7×10^{-4} cm² V⁻¹ s⁻¹) and morphology defects (some dots, see Figure 9d–f) of the active layer.

As shown in Figure 8, the incident photon-to-electron conversion efficiency (IPCE) curves are similar to their corresponding absorption spectra of blend films. P3:PC₇₁BM blend exhibits a narrower absorption spectrum (300–600 nm) and much lower

IPCE (below 4%), leading to much lower J_{sc} of 0.44 mA cm^{-2} . The P2:PC₇₁BM blend exhibits a broader absorption between 300 and 700 nm and broader IPCE spectrum with a maximum of ca. 25%, leading to higher J_{sc} of 3.3 mA cm^{-2} . The P4:PC₇₁BM blend also exhibits a broader absorption between 300 and 700 nm and broader IPCE spectrum with a maximum of ca. 45%, leading to the highest J_{sc} of 6.64 mA cm^{-2} .

To elucidate the origin for the big difference in photovoltaic performance across these polymers, we investigate blend film morphology using atomic force microscope (AFM) (Figure 9). First of all, the film smoothness is an important factor because a smooth surface induces better contact with the cathode. The root-mean-square (rms) roughness of P2–P4 blend film is 9.42, 1.60, and 3.82 nm, respectively. Upon increasing the planarity of

the polymer main chain, the blend exhibits increase in phase separation scale and roughness. P2:PC₇₁BM exhibits large phase separation with large roughness. The most planar backbone of P2 favors stronger π – π interchain interaction and stronger aggregation in the thin film, leading to coarse morphology and large phase separation when blending with PC₇₁BM. This large phase separation scale is not favorable for efficient exciton dissociation, leading to relatively low J_{sc} . As fill factor is determined by charge carriers reaching the electrodes in blend film, which is related to not only charge transport but also nanomorphology,² the low FF in P2-based device is also attributed to coarse morphology and large phase separation although P2 exhibits high mobility in its single-component film. Some dots in the P3:PC₇₁BM film span across the film, which might act as defects in the device and cause charge recombination. Thus, the low hole mobility and the morphology defects of the blend film lead to low J_{sc} and FF in P3-based device. The P4:PC₇₁BM film exhibits many aggregated domains with chainlike and cross-link features and a moderate roughness. The domain sizes estimated by cross-section profiles are tens of nanometers. This featured nanoscale phase separation could facilitate the diffusion and separation of excitons and charge transport, leading to the highest J_{sc} , FF, and PCE.

Table 4. Photovoltaic Performances of PSCs Based on P2–P4 under the Illumination of AM 1.5, 100 mW cm^{-2}

active layer	V_{oc} (V)	J_{sc} (mA cm^{-2})	FF (%)	PCE (%)
P2:PC ₇₁ BM = 1:1	0.91	3.30	37.8	1.14
P3:PC ₇₁ BM = 1:1	0.76	0.44	25.4	0.09
P4:PC ₇₁ BM = 1:1	0.82	6.64	46.6	2.54

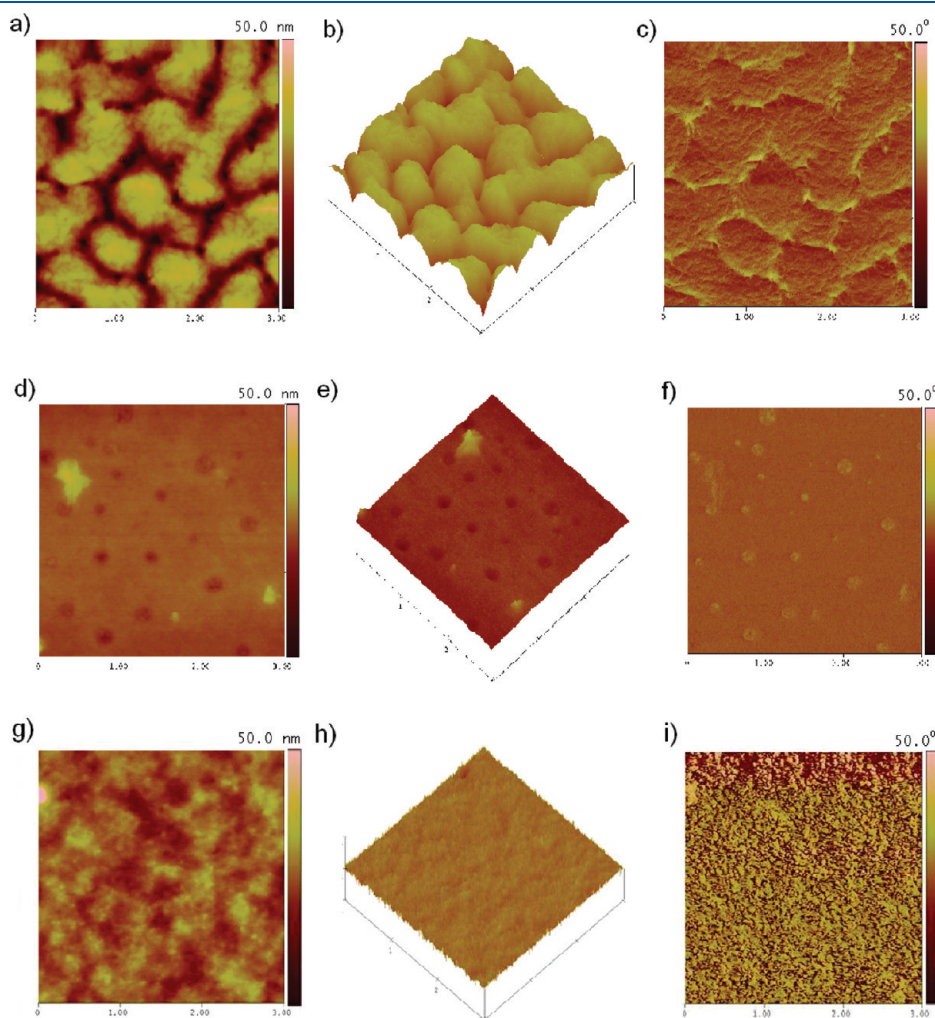


Figure 9. AFM topographic images ($3 \times 3 \mu\text{m}$) (left), 3D surface images (middle), and phase images (right) for thin films of blends of P2 (top), P3 (middle), and P4 (bottom) with PC₇₁BM (1:1, w/w).

CONCLUSIONS

Four copolymers **P1**–**P4** containing the same backbone of bithiazole acceptor unit and benzodithiophene donor unit but different side chain pattern were synthesized by the Pd-catalyzed Stille coupling. Slight difference in the side chain pattern leads to big difference in backbone conformation, solubility, absorption spectra, energy levels, charge transport, blend film morphology, and photovoltaic properties of the polymers. Because of the twisted structure of the main chain, **P3** exhibits relatively narrow absorption, large bandgap, low HOMO and high LUMO, low mobility, and poor photovoltaic properties. In sharp contrast to **P3**, **P2** and **P4** with the planar structures exhibit relatively broader absorption, smaller bandgap, and higher HOMO and lower LUMO. The most planar backbone of **P2** causes strong π – π interchain interaction and strong aggregation, leading to highest mobility, largest phase separation, and moderate PCE. Because of the moderate planarity of the main chain, **P4** exhibits combination of broad absorption, high mobility, and suitable phase separation, leading to the highest PCE. This work demonstrates a good example for tuning backbone conformation, absorption, energy level, charge transport, phase separation, and photovoltaic properties of the polymers by side chain engineering.

AUTHOR INFORMATION

Corresponding Author

*E-mail: xwzhan@iccas.ac.cn.

ACKNOWLEDGMENT

This work was supported by NSFC (Grants 21025418, 51011130028, 21021091), 973 Project (Grant 2011CB80-8400), and the Chinese Academy of Sciences.

REFERENCES

- (1) Coakley, K. M.; McGehee, M. D. *Chem. Mater.* **2004**, *16*, 4533.
- (2) Gunes, S.; Neugebauer, H.; Sariciftci, N. S. *Chem. Rev.* **2007**, *107*, 1324.
- (3) Bundgaard, E.; Krebs, F. C. *Sol. Energ. Mater. Sol. Cells* **2007**, *91*, 954.
- (4) Chen, J. W.; Cao, Y. *Acc. Chem. Res.* **2009**, *42*, 1709.
- (5) Cheng, Y. J.; Yang, S. H.; Hsu, C. S. *Chem. Rev.* **2009**, *109*, 5868.
- (6) Li, Y. F.; Zou, Y. P. *Adv. Mater.* **2008**, *20*, 2952.
- (7) Zhan, X. W.; Zhu, D. B. *Polym. Chem.* **2010**, *1*, 409.
- (8) He, Y. J.; Chen, H. Y.; Hou, J. H.; Li, Y. F. *J. Am. Chem. Soc.* **2010**, *132*, 5532.
- (9) Zhao, G. J.; He, Y. J.; Li, Y. F. *Adv. Mater.* **2010**, *22*, 4355.
- (10) Cheng, Y. J.; Hsieh, C. H.; He, Y. J.; Hsu, C. S.; Li, Y. F. *J. Am. Chem. Soc.* **2010**, *132*, 17381.
- (11) Chen, H. Y.; Hou, J. H.; Zhang, S. Q.; Liang, Y. Y.; Yang, G. W.; Yang, Y.; Yu, L. P.; Wu, Y.; Li, G. *Nature Photonics* **2009**, *3*, 649.
- (12) Szarko, J. M.; Guo, J.; Liang, Y.; Lee, B.; Rolczynski, B. S.; Strzalka, J.; Xu, T.; Loser, S.; Marks, T. J.; Yu, L.; Chen, L. X. *Adv. Mater.* **2010**, *22*, 5468.
- (13) Son, H. J.; Wang, W.; Xu, T.; Liang, Y. Y.; Wu, Y.; Li, G.; Yu, L. *J. Am. Chem. Soc.* **2011**, *133*, 1885.
- (14) Price, S. C.; Stuart, A. C.; Yang, L.; Zhou, H.; You, W. *J. Am. Chem. Soc.* **2011**, *133*, 4625.
- (15) Zhou, H.; Yang, L.; Stuart, A. C.; Price, S. C.; Liu, S.; You, W. *Angew. Chem., Int. Ed.* **2011**, *50*, 2995.
- (16) Chu, T. Y.; Lu, J.; Beaupré, S.; Zhang, Y.; Pouliot, J. R.; Wakim, S.; Zhou, J.; Leclerc, M.; Li, Z.; Ding, J.; Tao, Y. *J. Am. Chem. Soc.* **2011**, *133*, 4250.
- (17) Ando, S.; Murakami, R.; Nishida, J.; Tada, H.; Inoue, Y.; Tokito, S.; Yamashita, Y. *J. Am. Chem. Soc.* **2005**, *127*, 14996.
- (18) Liu, J. Y.; Zhang, R.; Osaka, I.; Mishra, S.; Javier, A. E.; Smilgies, D. M.; Kowalewski, T.; McCullough, R. D. *Adv. Funct. Mater.* **2009**, *19*, 3427.
- (19) Ie, Y.; Nitani, M.; Karakawa, M.; Tada, H.; Aso, Y. *Adv. Funct. Mater.* **2010**, *20*, 907.
- (20) Paek, S.; Lee, J.; Lim, H. S.; Lim, J.; Lee, J. Y.; Lee, C. *Synth. Met.* **2010**, *160*, 2273.
- (21) Lee, J.; Jung, B. J.; Lee, S. K.; Lee, J. I.; Cho, H. J.; Shim, H. K. *J. Polym. Sci., Part A: Polym. Chem.* **2005**, *43*, 1845.
- (22) Wong, W. Y.; Wang, X. Z.; He, Z.; Chan, K. K.; Djuricic, A. B.; Cheung, K. Y.; Yip, C. T.; Ng, A. M. C.; Xi, Y. Y.; Mak, C. S. K.; Chan, W. K. *J. Am. Chem. Soc.* **2007**, *129*, 14372.
- (23) Li, K. C.; Huang, J. H.; Hsu, Y. C.; Huang, P. J.; Chu, C. W.; Lin, J. T.; Ho, K. C.; Wei, K. H.; Lin, H. C. *Macromolecules* **2009**, *42*, 3681.
- (24) Huang, J. H.; Li, K. C.; Kekuda, D.; Padhy, H. H.; Lin, H. C.; Ho, K. C.; Chu, C. W. *J. Mater. Chem.* **2010**, *20*, 3295.
- (25) Jung, I. H.; Yu, J.; Jeong, E.; Kim, J.; Kwon, S.; Kong, H.; Lee, K.; Woo, H. Y.; Shim, H. K. *Chem.—Eur. J.* **2010**, *16*, 3743.
- (26) Patra, D.; Sahu, D.; Padhy, H.; Kekuda, D.; Chu, C. W.; Lin, H. C. *J. Polym. Sci., Part A: Polym. Chem.* **2010**, *48*, 5479.
- (27) Huang, J. H.; Li, K. C.; Chien, F. C.; Hsiao, Y. S.; Kekuda, D.; Chen, P. L.; Lin, H. C.; Ho, K. C.; Chu, C. W. *J. Phys. Chem. C* **2010**, *114*, 9062.
- (28) Zhang, M. J.; Fan, H. J.; Guo, X.; He, Y. J.; Zhang, Z. G.; Min, J.; Zhang, J.; Zhao, G. J.; Zhan, X. W.; Li, Y. F. *Macromolecules* **2010**, *43*, 5706.
- (29) Shi, Q. Q.; Fan, H. J.; Liu, Y.; Hu, W. P.; Li, Y. F.; Zhan, X. W. *J. Phys. Chem. C* **2010**, *114*, 16843.
- (30) Yang, M. A.; Peng, B.; Liu, B.; Zou, Y. P.; Zhou, K. C.; He, Y. H.; Pan, C. Y.; Li, Y. F. *J. Phys. Chem. C* **2010**, *114*, 17989.
- (31) Zhang, M. J.; Fan, H. J.; Guo, X.; He, Y. J.; Zhang, Z. G.; Min, J.; Zhang, J.; Zhao, G. J.; Zhan, X. W.; Li, Y. F. *Macromolecules* **2010**, *43*, 8714.
- (32) Adam, G.; Pivrikas, A.; Ramil, A. M.; Tadesse, S.; Yohannes, T.; Sariciftci, N. S.; Egbe, D. A. M. *J. Mater. Chem.* **2011**, *21*, 2594.
- (33) Price, S. C.; Stuart, A. C.; You, W. *Macromolecules* **2010**, *43*, 797.
- (34) Zhou, H. X.; Yang, L. Q.; Xiao, S. Q.; Liu, S. B.; You, W. *Macromolecules* **2010**, *43*, 811.
- (35) Yang, L. Q.; Zhou, H. X.; You, W. *J. Phys. Chem. C* **2010**, *114*, 16793.
- (36) Biniek, L.; Fall, S.; Chochos, C. L.; Anokhin, D. V.; Ivanov, D. A.; Leclerc, N.; Lévêque, P.; Heiser, T. *Macromolecules* **2010**, *43*, 9779.
- (37) Mondal, R.; Ko, S. W.; Verploegen, E.; Becerril, H. A.; Toney, M. F.; Bao, Z. *J. Mater. Chem.* **2011**, *21*, 1537.
- (38) Ho, V.; Boudouris, B. W.; Segalman, R. A. *Macromolecules* **2010**, *43*, 7895.
- (39) Tu, G. L.; Massip, S.; Oberhumer, P. M.; He, X. M.; Friend, R. H.; Greenham, N. C.; Huck, W. T. S. *J. Mater. Chem.* **2010**, *20*, 9231.
- (40) Friedel, B.; McNeill, C. R.; Greenham, N. C. *Chem. Mater.* **2010**, *22*, 3389.
- (41) Zoombelt, A. P.; Leenen, M. A. M.; Fonrodona, M.; Nicolas, Y.; Wienk, M. M.; Janssen, R. A. J. *Polymer* **2009**, *50*, 4564.
- (42) Zhang, S. M.; Guo, Y. L.; Fan, H. J.; Liu, Y.; Chen, H. Y.; Yang, G. W.; Zhan, X. W.; Liu, Y. Q.; Li, Y. F.; Yang, Y. J. *Polym. Sci., Part A: Polym. Chem.* **2009**, *47*, 5498.
- (43) Fan, H. J.; Zhang, Z. G.; Li, Y. F.; Zhan, X. W. *J. Polym. Sci., Part A: Polym. Chem.* **2011**, *49*, 1462.
- (44) Mayer, A. C.; Toney, M. F.; Scully, S. R.; Rivnay, J.; Brabec, C. J.; Scharber, M.; Koppe, M.; Heeney, M.; McCulloch, L.; McGehee, M. D. *Adv. Funct. Mater.* **2009**, *19*, 1173.
- (45) Muller, C.; Ferenczi, T. A. M.; Campoy-Quiles, M.; Frost, J. M.; Bradley, D. D. C.; Smith, P.; Stingelin-Stutzmann, N.; Nelson, J. *Adv. Mater.* **2008**, *20*, 3510.

- (46) Cates, N. C.; Gysel, R.; Dahl, J. E. P.; Sellinger, A.; McGehee, M. D. *Chem. Mater.* **2010**, *22*, 3543.
- (47) Johns, J. E.; Muller, E. A.; Frechet, J. M. J.; Harris, C. B. *J. Am. Chem. Soc.* **2010**, *132*, 15720.
- (48) Cates, N. C.; Gysel, R.; Beiley, Z.; Miller, C. E.; Toney, M. F.; Heeney, M.; McCulloch, I.; McGehee, M. D. *Nano Lett.* **2009**, *9*, 4153.
- (49) Li, W. W.; Qin, R. P.; Zhou, Y.; Andersson, M.; Li, F. H.; Zhang, C.; Li, B. S.; Liu, Z. P.; Bo, Z. S.; Zhang, F. L. *Polymer* **2010**, *51*, 3031.
- (50) Kim, J. S.; Lee, Y.; Lee, J. H.; Park, J. H.; Kim, J. K.; Cho, K. *Adv. Mater.* **2010**, *22*, 1355.
- (51) Hollinger, J.; Jahnke, A. A.; Coombs, N.; Seferos, D. S. *J. Am. Chem. Soc.* **2010**, *132*, 8546.
- (52) Hou, J. H.; Park, M. H.; Zhang, S. Q.; Yao, Y.; Chen, L. M.; Li, J. H.; Yang, Y. *Macromolecules* **2008**, *41*, 6012.
- (53) Hagemann, O.; Jorgensen, M.; Krebs, F. C. *J. Org. Chem.* **2006**, *71*, 5546.
- (54) Sato, T.; Kishida, H.; Nakamura, A.; Fukuda, T.; Yamamoto, T. *Synth. Met.* **2007**, *157*, 318.
- (55) Pommerehne, J.; Vestweber, H.; Guss, W.; Mahrt, R. F.; Bassler, H.; Porsch, M.; Daub, J. *Adv. Mater.* **1995**, *7*, 551.
- (56) Becke, A. D. *J. Chem. Phys.* **1993**, *98*, 5648.
- (57) Lee, C. T.; Yang, W. T.; Parr, R. G. *Phys. Rev. B* **1988**, *87*, 785.
- (58) Gaussian 09, Revision A.1: Frisch, M. J.; Trucks, G. W.; Schlegel, H. B.; Scuseria, G. E.; Robb, M. A.; Cheeseman, J. R.; Scalmani, G.; Barone, V.; Mennucci, B.; Petersson, G. A.; Nakatsuji, H.; Caricato, M.; Li, X.; Hratchian, H. P.; Izmaylov, A. F.; Bloino, J.; Zheng, G.; Sonnenberg, J. L.; Hada, M.; Ehara, M.; Toyota, K.; Fukuda, R.; Hasegawa, J.; Ishida, M.; Nakajima, T.; Honda, Y.; Kitao, O.; Nakai, H.; Vreven, T.; Montgomery, Jr., J. A.; Peralta, J. E.; Ogliaro, F.; Bearpark, M.; Heyd, J. J.; Brothers, E.; Kudin, K. N.; Staroverov, V. N.; Kobayashi, R.; Normand, J.; Raghavachari, K.; Rendell, A.; Burant, J. C.; Iyengar, S. S.; Tomasi, J.; Cossi, M.; Rega, N.; Millam, J. M.; Klene, M.; Knox, J. E.; Cross, J. B.; Bakken, V.; Adamo, C.; Jaramillo, J.; Gomperts, R.; Stratmann, R. E.; Yazyev, O.; Austin, A. J.; Cammi, R.; Pomelli, C.; Ochterski, J. W.; Martin, R. L.; Morokuma, K.; Zakrzewski, V. G.; Voth, G. A.; Salvador, P.; Dannenberg, J. J.; Dapprich, S.; Daniels, A. D.; Farkas, Ö.; Foresman, J. B.; V. Ortiz, J.; Cioslowski, J.; Fox, D. J. Gaussian, Inc.: Wallingford, CT, 2009.
- (59) Anthony, J. E.; Facchetti, A.; Heeney, M.; Marder, S. R.; Zhan, X. W. *Adv. Mater.* **2010**, *22*, 3876.
- (60) Li, Z.; Ding, J.; Song, N.; Du, X.; Zhou, J.; Lu, J.; Tao, Y. *Chem. Mater.* **2011**, *23*, 1977.
- (61) Scharber, M. C.; Wuhlbacher, D.; Koppe, M.; Denk, P.; Waldauf, C.; Heeger, A. J.; Brabec, C. L. *Adv. Mater.* **2006**, *18*, 789.
- (62) Xiao, S. Q.; Stuart, A. C.; Liu, S. B.; Zhou, H. X.; You, W. *Adv. Funct. Mater.* **2010**, *20*, 635.